

# Shubnikov-de Haas and de Haas-van Alphen oscillations in topological semimetal CaAl<sub>4</sub>

Sheng Xu,\* Jian-Feng Zhang,\* Yi-Yan Wang<sup>†</sup>,\* Lin-Lin Sun<sup>‡</sup>, Huan

Wang, Yuan Su, Xiao-Yan Wang, Kai Liu, and Tian-Long Xia<sup>§</sup>

*Department of Physics, Renmin University of China, Beijing 100872, P. R. China and  
Beijing Key Laboratory of Opto-electronic Functional Materials & Micro-nano Devices,*

*Renmin University of China, Beijing 100872, P. R. China*

(Dated: March 17, 2022)

We report the magneto-transport properties of CaAl<sub>4</sub> single crystals with  $C2/m$  structure at low temperature. CaAl<sub>4</sub> exhibits large unsaturated magnetoresistance  $\sim 3000\%$  at 2.5 K and 14 T. The nonlinear Hall resistivity is observed, which indicates the multi-band feature. The first-principles calculations show the electron-hole compensation and the complex Fermi surface in CaAl<sub>4</sub>, to which the two-band model with over-simplified carrier mobility can't completely apply. Evident quantum oscillations have been observed with B//c and B//ab configurations, from which the nontrivial Berry phase is extracted by the multi-band Lifshitz-Kosevich formula fitting. An electron-type quasi-2D Fermi surface is found by the angle-dependent Shubnikov-de Haas oscillations, de Haas-van Alphen oscillations and the first-principles calculations. The calculations also elucidate that CaAl<sub>4</sub> owns a Dirac nodal line type band structure around the  $\Gamma$  point in the  $Z-\Gamma-L$  plane, which is protected by the mirror symmetry as well as the space inversion and time reversal symmetries. Once the spin-orbit coupling is included, the crossed nodal line opens a negligible gap (less than 3 meV). The open-orbit topology is also found in the electron-type Fermi surfaces, which is believed to help enhance the magnetoresistance observed.

## I. INTRODUCTION

Topological semimetals have been a recent research focus due to their novel properties in condensed matter physics. Dirac semimetals display a four-fold degenerate Dirac point with two linear crossing bands<sup>1</sup>. Cd<sub>3</sub>As<sub>2</sub><sup>2-7</sup> and Na<sub>3</sub>Bi<sup>8-11</sup> are the typical Dirac semimetals. Once the space inversion or time reversal symmetry is broken, the Dirac semimetals will evolve into Weyl semimetals<sup>12,13</sup> like TaAs family<sup>14-25</sup> or SrMnSb<sub>2</sub>/YbMnPn<sub>2</sub> (Pn= Sb and Bi)<sup>26-29</sup>. Different from the Dirac and Weyl semimetals, PbTaSe<sub>2</sub><sup>30</sup> and ZrSiS family<sup>31-33</sup> possess a one-dimensional loop band touching, which are known as the nodal-line semimetals<sup>34</sup>. All of these topological semimetals have demonstrated interesting transport properties. Lately, transition-metal dipnictides XPn<sub>2</sub> (X=Nb or Ta; Pn= As or Sb) with  $C2/m$  structure have attracted tremendous attention due to the novel phenomena such as resistivity plateau, extremely large magnetoresistance (MR) and negative longitudinal MR *etc.*<sup>35-40</sup>. It is believed that the extremely large MR in XPn<sub>2</sub> may originate from the electron-hole compensation, while the other mechanism may enhance it<sup>35-42</sup>.

Motivated by previous results and discussions, we grew the high-quality CaAl<sub>4</sub> single crystals with the space group  $C2/m$  at room temperature and studied its transport properties and electronic structure in details. The first-principles calculations reveal that there is a Dirac nodal line around the  $\Gamma$  point in the  $Z-\Gamma-L$  plane, which is protected by the mirror symmetry as well as the space inversion and time reversal symmetries. However, the crossed nodal line opens a negligible gap (less than 3 meV) once the spin-orbit coupling (SOC) is included. Interestingly, an electron-type quasi-2D Fermi

surface (FS) is observed, which plays an important role in the magneto-transport properties. Magneto-transport measurements on CaAl<sub>4</sub> display a large unsaturated MR up to 3000% at 2.5 K and 14 T. The nonlinear and negative Hall resistivity indicate the multi-band and electron dominant features, which is slightly in disagreement with the calculations. According to the analysis of the two-band model, the electron-hole un-compensation is expected, while the calculations suggest that the electron and hole are compensated. The mismatch is discussed in the main text of this paper. Besides, evident Haas-van Alphen oscillations (dHvA) and Shubnikov-de Haas oscillations (SdH) have been observed at low temperature and high magnetic field. Three fundamental frequencies have been extracted after the fast Fourier transform (FFT) analysis with B//c configuration. The multi-band Lifshitz-Kosevich (LK) formula fitting yields the nontrivial Berry phase. Angle-dependent SdH oscillations reveal that the  $\gamma$  pocket displays quasi-2D characteristic which is in agreement with the calculations.

## II. METHODS AND CRYSTAL STRUCTURE

The high quality single crystals of CaAl<sub>4</sub> were grown by the self-flux method. The calcium and aluminum granules were put into the crucible and sealed into a quartz tube with the ratio Ca:Al=14:86. The quartz tube was heated to 900°C, then cooled to 690°C in 70 hours, and to 660°C in 30 hours. The excess flux was removed by centrifugation. The atomic composition of CaAl<sub>4</sub> single crystal was checked to be Ca:Al=1:4 by energy dispersive x-ray spectroscopy (EDS, Oxford X-Max 50). The single-crystal x-ray diffraction (XRD) pattern and temperature dependent powder XRD patterns were collected from a Bruker D8 Advance x-ray diffractometer using Cu  $K_{\alpha}$  radiation. TOPAS-4.2 was employed for the refinement. The measurements of resistivity and magnetic properties were performed on a Quantum Design physical property

<sup>†</sup>Present address: Institute of Physics, Chinese Academy of Sciences.

<sup>‡</sup>Present address: Pinggu Branch of High School Affiliated to Beijing Normal University.

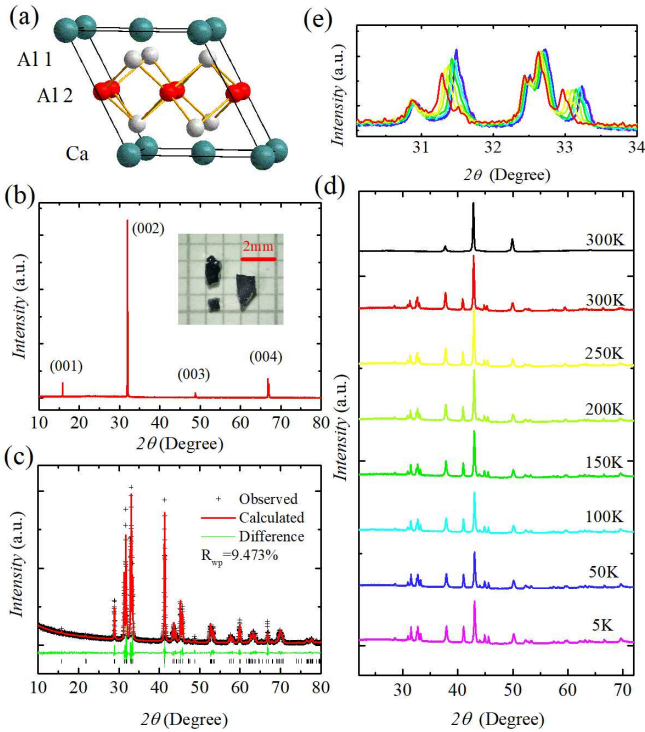


FIG. 1: (a) Crystal structure of  $\text{CaAl}_4$  at room temperature. (b) Single crystal XRD pattern of  $\text{CaAl}_4$  at room temperature. Inset shows the picture of selected crystals. (c) Powder XRD pattern and the Rietveld refinement of  $\text{CaAl}_4$ . The value of  $R_{wp}$  is 9.413%. (d), (e) Powder XRD patterns and the enlargement part of  $\text{CaAl}_4$  with the background of the platform (The curve in black at 300 K) at different temperatures.

measurement system (QD PPMS-14T). The electronic structure was studied by the first-principles calculations with the projector augmented wave (PAW) method<sup>43,44</sup> as implemented in the VASP package<sup>45-47</sup>. For the exchange-correlation functional, the generalized gradient approximation (GGA) of the Perdew-Burke-Ernzerhof (PBE) formula<sup>48</sup> was adopted. The kinetic energy cutoff of the plane-wave basis was set to be 350 eV. A  $20 \times 20 \times 20$   $k$ -point mesh was utilized for the BZ sampling and the Fermi surface was broadened by the Gaussian smearing method with a width of 0.05 eV. The lattice parameters and internal atomic positions were fully relaxed until the forces on all atoms were smaller than 0.01 eV/Å. After the equilibrium structures were obtained, the electronic structures were calculated by including the SOC effect. The Fermi surfaces were studied by using the maximally localized Wannier functions (MLWF) method<sup>49,50</sup>.

The crystal structure of  $\text{CaAl}_4$  is reported to be  $I4/mmm$  in the ICSD database. However, Miller *et al.* pointed out its structure transition from tetragonal to monoclinic at 443 K<sup>51</sup> and its room temperature structure is  $C2/m$ <sup>51</sup> which is the same as that of  $\text{XPn}_2$  family. Figure 1(b) shows the XRD pattern of a single crystal at room temperature, which reveals the surface of the crystal is the (00 $l$ ) plane. The powder XRD pattern (the sample is crushed from the single crystals) is also checked and shown in Fig. 1(c) which can be well re-

finied with  $C2/m$  (No.12) space group. The refined lattice parameters are  $a = 6.1695\text{Å}$ ,  $b = 6.1842\text{Å}$ ,  $c = 6.3451\text{Å}$  and  $\beta = 118.0647^\circ$ , which are in agreement with previous results<sup>51</sup>. In addition, the Young modulus indicated that there may exist another structure transition at  $\sim 243\text{ K}$ <sup>52</sup>. Thus, we performed the temperature dependent XRD measurements on  $\text{CaAl}_4$  powder sample between 300 K and 5 K as shown in Figs. 1(d) and 1(e). The black line in Fig. 1(d) shows the XRD pattern of the sample platform at 300 K. The temperature dependent powder diffraction pattern does not change obviously [Fig. 1(e)], in which only the peak position of the specific crystal plane changes slightly to the higher  $2\theta$  value with the decreasing temperature [Fig. 1(e)], which originates from the decrease of the lattice parameters. Thus, there is no structure transition among this temperature range.

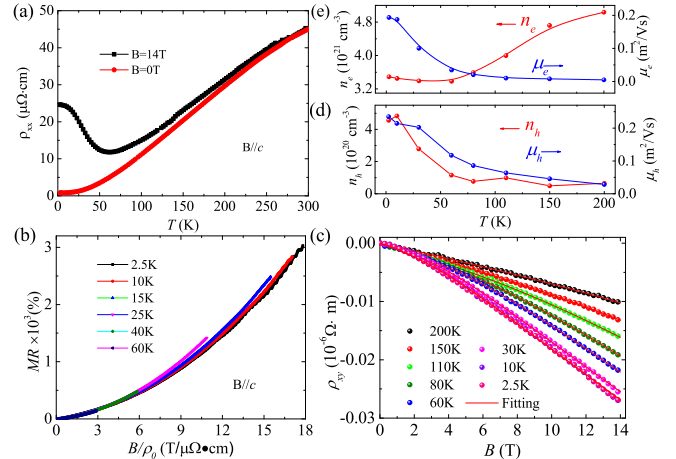


FIG. 2: (a) Temperature dependent resistivity of  $\text{CaAl}_4$  at 0 T and 14 T. (b) The plot of MR as a function of  $B/\rho_0$  at different temperatures. (c) Magnetic field dependent Hall resistivity at various temperatures. The red lines are the fitting results from the two-band model. (d), (e) Temperature dependence of carrier concentrations and mobility.

### III. RESULTS AND DISCUSSIONS

Figure 2(a) exhibits the temperature dependent resistivity  $\rho_{xx}(0)$  and  $\rho_{xx}(14T)$ . The  $\rho_{xx}(0)$  shows metallic behaviour and the residual resistance ratio (RRR) equal to 57. The resistivity  $\rho_{xx}(14T)$  shows an upturn below 60 K accompanied with a plateau. Figure 2(b) plots the magnetic field dependent MR at various temperatures when  $B$  is applied parallel to  $c$ -axis. The MR reaches 3000% at 2.5 K and 14 T which is comparable to that of type-II Weyl semimetal  $\text{Ta}_3\text{S}_2$ <sup>53</sup>. The MR in Fig. 2(b) shows  $B^{1.6}$  field dependence which violates the Kohler's rule, indicating the coexistence of electrons and holes<sup>54</sup>. In order to thoroughly identify the characteristics of the carriers in  $\text{CaAl}_4$ , we performed temperature dependent Hall resistivity measurements. The Hall resistivity  $\rho_{xy}$  curves of  $\text{CaAl}_4$  at various temperatures from 2.5 K to 200 K are shown in Fig. 2(c). The two-band model is used to describe the Hall resistivity,

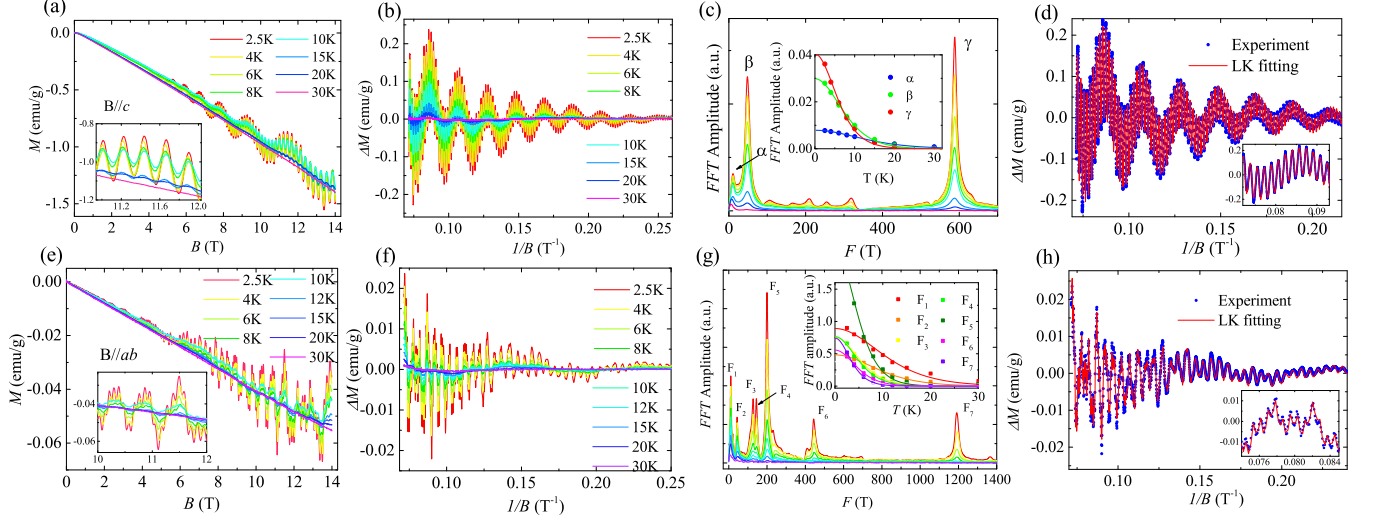


FIG. 3: (a), (e) The dHvA oscillations at various temperatures for  $B//c$  and  $B//ab$ . (b), (f) The amplitudes of dHvA oscillations as a function of  $1/B$ . (c), (g) The FFT spectra of the oscillations. The insets are the temperature dependence of relative FFT amplitude of the main oscillation frequency. (d), (h) The fitting of dHvA oscillations at 2.5 K by the multi-band LK formula.

$$\rho_{xy} = \frac{B}{e} \frac{(n_h \mu_h^2 - n_e \mu_e^2) + (n_h - n_e)(\mu_h \mu_e)^2 B^2}{(n_h \mu_h + n_e \mu_e)^2 + (n_h - n_e)^2 (\mu_h \mu_e)^2 B^2} \quad (1)$$

where  $n_{e,h}$  and  $\mu_{e,h}$  represent the concentration and mobility of electrons and holes, respectively. The red lines in Fig. 2(c) are the fitting results, and the temperature dependent concentrations and mobility are plotted in Figs. 2(d) and 2(e). At 2.5 K,  $n_e = 3.5 \times 10^{21} \text{cm}^{-3}$  and it is almost eight times larger than  $n_h = 4.5 \times 10^{20} \text{cm}^{-3}$ , and the  $\mu_e$  and  $\mu_h$  are  $0.19 \text{m}^2/\text{V}^{-1}\text{s}^{-1}$  and  $0.23 \text{m}^2/\text{V}^{-1}\text{s}^{-1}$ , respectively. Nevertheless, the first-principles calculations indicate that the electron and hole are compensated with the concentrations  $n_e \approx n_h = 1 \times 10^{21} \text{cm}^{-3}$ . Both the quantum oscillations and the calculations confirmed the multi-band character in  $\text{CaAl}_4$ , each of which shows different mobility. However, the two-band model simplified the mobility into a simple one  $\mu_e \mu_h$ , which leads to the disagreement of concentrations between the fitting and the calculations.

Quantum oscillation experiment is an effective method in the study of topological materials.  $\text{CaAl}_4$  shows obvious dHvA oscillations, as shown in Figs. 3(a) and 3(e) with magnetic field up to 14 T. The dHvA oscillations are more distinct at lower temperature and higher field. After subtracting a smoothing background, the periodic oscillations  $\Delta M = M - \langle M \rangle$  versus  $1/B$  are shown in Fig. 3(b) for  $B//c$  and 3(f) for  $B//ab$ , respectively. Three fundamental frequencies  $F_\alpha = 10.7$  T,  $F_\beta = 48.4$  T and  $F_\gamma = 588.3$  T are obtained after the FFT analysis when the field is applied along c-axis. The number of FFT frequencies almost doubles when the field is applied along the ab-plane as presented in Table I, indicating the more complex FS cross sections along this direction. The oscillatory components versus  $1/B$  of dHvA oscillations can be described by the LK formula<sup>55</sup>:

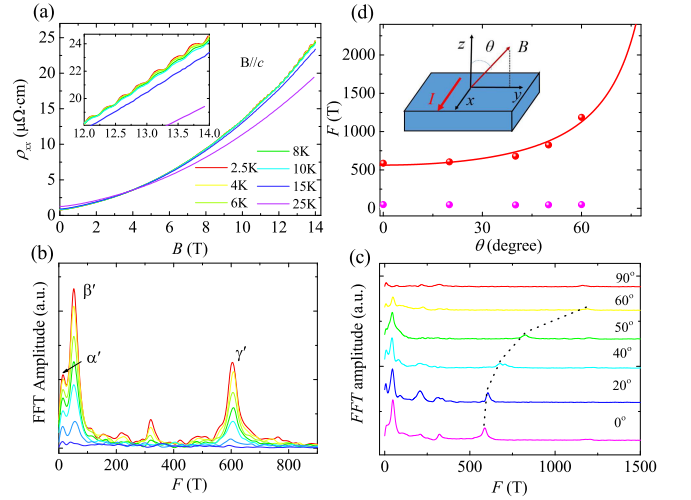


FIG. 4: (a) Resistivity  $\rho_{xx}(B)$  as a function of field ( $B//c$ ) at various temperatures. Inset shows the enlargement of the oscillations at high field. (b) The FFT spectra of SdH oscillations at different temperatures. (c) The FFT spectra of SdH oscillations with the field in different directions at 2.5 K. (d) Angle dependence of the frequencies. The solid line in red is the fitting curve with  $F = F_0/\cos(\theta)$  for  $\gamma'$  pocket. The inset shows the definition of  $\theta$ .

$$\Delta M \propto -B^{1/2} \frac{\lambda T}{\sinh(\lambda T)} e^{-\lambda T_D} \sin\left[2\pi\left(\frac{F}{B} - \frac{1}{2} + \beta + \delta\right)\right] \quad (2)$$

where  $\lambda = (2\pi^2 k_B m^*)/(\hbar e B)$ .  $T_D$  is the Dingle temperature. The value of  $\delta$  depends on the dimensionality,  $\delta = 0$  for the 2D system and  $\delta = \pm 1/8$  for the 3D system.  $\beta = \phi_B/2\pi$  and  $\phi_B$  is the Berry phase. The insets of Figs. 3(c) and 3(g) show the temperature dependent FFT amplitudes and the fitting by the thermal factor  $R_T = (\lambda T)/\sinh(\lambda T)$  in LK

TABLE I: The parameters extracted from dHvA oscillations in CaAl<sub>4</sub>. F is the frequency of dHvA oscillations;  $m^*/m_e$  is the ratio of the effective mass to the electron mass;  $\phi_B$  is the Berry phase.

	F(T)	$m^*/m_e$	$\phi_B(\delta=0)$	$\phi_B(\delta=-1/8)$	$\phi_B(\delta=1/8)$	
B//c	$\alpha$	10.7	0.07	/	$1.15\pi$	
	$\beta$	48.4	0.12	/	$0.34\pi$	
	$\gamma$	588.3	0.15	$1.65\pi$	/	
B//ab	F <sub>1</sub>	10.9	0.06	/	$1.57\pi$	
	F <sub>2</sub>	43.7	0.07	/	$0.57\pi$	
	F <sub>3</sub>	127.5	0.13	$0.06\pi$	$0.31\pi$	$-0.19\pi$
	F <sub>4</sub>	144.5	0.14	$1.61\pi$	$1.86\pi$	$1.36\pi$
	F <sub>5</sub>	200.2	0.14	$1.62\pi$	$1.87\pi$	$1.37\pi$
	F <sub>6</sub>	444.5	0.15	$1.39\pi$	$1.63\pi$	$1.13\pi$
	F <sub>7</sub>	1192.5	0.20	$0.87\pi$	$1.12\pi$	$0.62\pi$

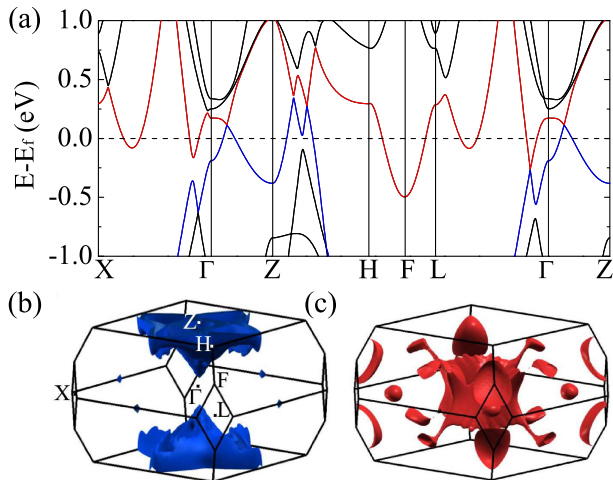


FIG. 5: (color online) (a) The band structure of CaAl<sub>4</sub> with SOC considered. (b),(c) The hole-like and electron-like Fermi surfaces of CaAl<sub>4</sub>.

formula, from which the effective masses are obtained to be  $m_\alpha^* = 0.07m_e$ ,  $m_\beta^* = 0.12m_e$  and  $m_\gamma^* = 0.15m_e$  (B//c). As is well known, topological non-trivial materials require a non-trivial  $\pi$  Berry phase, while for the trivial materials, the Berry phase equals 0 or  $2\pi$ . In this work, it is a challenge to employ Landau level (LL) index fan diagram analysis since the oscillations contain too many frequencies. Thus, we applied multi-band LK formula fitting as displayed in Figs. 3(d) and 3(h). The obtained Berry phases of each pocket are exhibited in Table I, several of which are close to  $\pi$  indicating the possible topological non-trivial characteristic.

Figure 4(a) displays  $\rho_{xx}(B)$  versus magnetic field at various temperatures. The CaAl<sub>4</sub> exhibits obvious SdH oscillations at low temperature and high field (B//c). The oscillations tend to disappear with the increasing temperature and almost vanish at 25 K. Fig. 4(b) shows the FFT frequencies  $F'_\alpha=6.3$  T,  $F'_\beta=53$  T and  $F'_\gamma=605$  T of the SdH oscillations. The effective masses of these pockets are extracted to be  $m_{F'_\alpha}^* = 0.07m_e$ ,  $m_{F'_\beta}^* = 0.12m_e$  and  $m_{F'_\gamma}^* = 0.13m_e$ . Both the FFT frequencies and the relevant effective masses are comparable to that of dHvA oscillations with B//c configuration. In order to study

its electronic structure in details, we applied angle-dependent SdH oscillation measurements. The rotation angle is defined as  $\theta=0^\circ$  for B//c,  $\theta=90^\circ$  for B//ab and B is always perpendicular to the current I as shown in the insert of the Fig. 4(d). Figure 4(c) displays the FFT frequencies extracted from the SdH oscillations at different orientations.  $F'_\gamma$  shows an obvious angle dependent characteristic and is fitted by  $F=A/\cos(\theta)$  as shown in Fig. 4(c), which implies the quasi-2D FS morphology.

The electronic structure of CaAl<sub>4</sub> with SOC is calculated and presented in Fig. 5(a). The first-principles calculations elucidate that CaAl<sub>4</sub> owns a Dirac nodal line around the  $\Gamma$  point in the  $Z$ - $\Gamma$ - $L$  plane, which is protected by the mirror symmetry as well as the space inversion and time reversal symmetries. When the SOC is considered, the crossed nodal line opens a negligible gap which is less than 3 meV. This negligible gap almost has no effect on the topological properties, especially in the magneto-transport measurements. Figures 5(b) and 5(c) display the hole-type and electron-type FSs, respectively, where the electron-type FSs contain a quasi-2D FS [Fig. 5(c)] which coincides with the result of the transport measurements.

#### IV. SUMMARY

In conclusion, we synthesized the single crystals of CaAl<sub>4</sub> and confirmed its crystal structure as  $C2/m$  at low temperature. The possible secondary structure transition at  $\sim 243$  K indicated in previous results is not observed. The large MR reaches  $\sim 3000\%$  at 2.5 K and 14 T. The multi-band feature is revealed by the analysis of Hall resistivity and the first-principles calculations. The disagreement between the two-band model fitting and the calculations comes from the oversimplified model. Evident dHvA oscillations have been observed, from which the nontrivial Berry phase is extracted from the multi-band LK formula fitting. CaAl<sub>4</sub> possesses a Dirac nodal ring type band structure around  $\Gamma$  point, which is protected by the mirror symmetry as well as the space inversion and time reversal symmetries. The crossed nodal line opens a negligible gap (less than 3 meV) when the SOC is included, which almost has no influence on the topological properties in the magneto-transport measurements. A quasi-2D electron-type FS is found by the angle-dependent SdH oscillations, in agreement with the calculations. The carrier compensation and topological nontrivial bands with high carrier mobility are believed to result in the large MR in CaAl<sub>4</sub>, while the observed open-orbit topology in part of the quasi-2D Fermi surface helps enhance it.

#### V. ACKNOWLEDGMENTS

We thank Peng-Jie Guo for helpful discussions. This work is supported by the National Natural Science Foundation of China (No.11574391, No.11874422, No.11774424), the Fundamental Research Funds for the Central Universities, and the Research Funds of Renmin University of China

(No.18XNLG14). Computational resources have been provided by the Physical Laboratory of High Performance Com-

puting at Renmin University of China. The Fermi surfaces were prepared with the XCRYSDEN program<sup>56</sup>.

\* These authors contributed equally to this paper

<sup>§</sup> Electronic address: tlxia@ruc.edu.cn

- <sup>1</sup> T. Wehling, A. M. Black-Schaffer, and A. V. Balatsky, *Adv. Phys.* **63**, 1 (2014).
- <sup>2</sup> M. Neupane, S.-Y. Xu, R. Sankar, N. Alidoust, G. Bian, C. Liu, I. Belopolski, T.-R. Chang, H.-T. Jeng, H. Lin, *et al.*, *Nat. Commun.* **5**, 3786 (2014).
- <sup>3</sup> Z. Liu, J. Jiang, B. Zhou, Z. Wang, Y. Zhang, H. Weng, D. Prabhakaran, S. Mo, H. Peng, P. Dudin, *et al.*, *Nat. Mater.* **13**, 677 (2014).
- <sup>4</sup> S. Borisenko, Q. Gibson, D. Evtushinsky, V. Zabolotnyy, B. Büchner, and R. J. Cava, *Phys. Rev. Lett.* **113**, 027603 (2014).
- <sup>5</sup> T. Liang, Q. Gibson, M. N. Ali, M. Liu, R. Cava, and N. Ong, *Nat. Mater.* **14**, 280 (2015).
- <sup>6</sup> C.-Z. Li, L.-X. Wang, H. Liu, J. Wang, Z.-M. Liao, and D.-P. Yu, *Nat. Commun.* **6**, 10137 (2015).
- <sup>7</sup> H. Li, H. He, H. Lu, H. Zhang, H. Liu, R. Ma, Z. Fan, S. Shen, and J. Wang, *Nat. Commun.* **7**, 10301 (2015).
- <sup>8</sup> Z. Wang, Y. Sun, X.-Q. Chen, C. Franchini, G. Xu, H. Weng, X. Dai, and Z. Fang, *Phys. Rev. B* **85**, 195320 (2012).
- <sup>9</sup> Z. Liu, B. Zhou, Y. Zhang, Z. Wang, H. Weng, D. Prabhakaran, S.-K. Mo, Z. Shen, Z. Fang, X. Dai, *et al.*, *Science* **343**, 864 (2014).
- <sup>10</sup> J. Xiong, S. K. Kushwaha, T. Liang, J. W. Krizan, M. Hirschberger, W. Wang, R. Cava, and N. Ong, *Science* **350**, 413 (2015).
- <sup>11</sup> J. Xiong, S. Kushwaha, J. Krizan, T. Liang, R. Cava, and N. Ong, *EPL* **114**, 27002 (2016).
- <sup>12</sup> X. Wan, A. M. Turner, A. Vishwanath, and S. Y. Savrasov, *Phys. Rev. B* **83**, 205101 (2011).
- <sup>13</sup> Z. Fang, N. Nagaosa, K. S. Takahashi, A. Asamitsu, R. Mathieu, T. Ogasawara, H. Yamada, M. Kawasaki, Y. Tokura, and K. Terakura, *Science* **302**, 92 (2003).
- <sup>14</sup> H. Weng, C. Fang, Z. Fang, B. A. Bernevig, and X. Dai, *Phys. Rev. X* **5**, 011029 (2015).
- <sup>15</sup> S.-Y. Xu, I. Belopolski, N. Alidoust, M. Neupane, G. Bian, C. Zhang, R. Sankar, G. Chang, Z. Yuan, C.-C. Lee, *et al.*, *Science* **349**, 613 (2015).
- <sup>16</sup> S.-M. Huang, S.-Y. Xu, I. Belopolski, C.-C. Lee, G. Chang, B. Wang, N. Alidoust, G. Bian, M. Neupane, C. Zhang, *et al.*, *Nat. Commun.* **6**, 7373 (2015).
- <sup>17</sup> B. Lv, H. Weng, B. Fu, X. Wang, H. Miao, J. Ma, P. Richard, X. Huang, L. Zhao, G. Chen, *et al.*, *Phys. Rev. X* **5**, 031013 (2015).
- <sup>18</sup> B. Q. Lv, N. Xu, H. M. Weng, J. Z. Ma, P. Richard, X. C. Huang, L. X. Zhao, G. F. Chen, C. E. Matt, F. Bisti, V. N. Strocov, J. Mesot, Z. Fang, X. Dai, T. Qian, M. Shi, and H. Ding, *Nat. Phys.* **11**, 724 (2015).
- <sup>19</sup> S.-Y. Xu, N. Alidoust, I. Belopolski, Z. Yuan, G. Bian, T.-R. Chang, H. Zheng, V. N. Strocov, D. S. Sanchez, G. Chang, *et al.*, *Nat. Phys.* **11**, 748 (2015).
- <sup>20</sup> S.-Y. Xu, I. Belopolski, D. S. Sanchez, C. Zhang, G. Chang, C. Guo, G. Bian, Z. Yuan, H. Lu, T.-R. Chang, *et al.*, *Sci. Adv.* **1**, e1501092 (2015).
- <sup>21</sup> N. Xu, H. Weng, B. Lv, C. Matt, J. Park, F. Bisti, V. Strocov, D. Gawryluk, E. Pomjakushina, K. Conder, *et al.*, *Nat. Commun.* **7** (2016).
- <sup>22</sup> Z. Liu, L. Yang, Y. Sun, T. Zhang, H. Peng, H. Yang, C. Chen, Y. Zhang, Y. f Guo, D. Prabhakaran, *et al.*, *Nat. Mater.* **15**, 27 (2016).
- <sup>23</sup> X. Huang, L. Zhao, Y. Long, P. Wang, D. Chen, Z. Yang, H. Liang, M. Xue, H. Weng, Z. Fang, *et al.*, *Phys. Rev. X* **5**, 031023 (2015).
- <sup>24</sup> C.-L. Zhang, S.-Y. Xu, I. Belopolski, Z. Yuan, Z. Lin, B. Tong, G. Bian, N. Alidoust, C.-C. Lee, S.-M. Huang, *et al.*, *Nat. Commun.* **7** (2016).
- <sup>25</sup> F. Arnold, C. Shekhar, S.-C. Wu, Y. Sun, R. D. Dos Reis, N. Kumar, M. Naumann, M. O. Ajeesh, M. Schmidt, A. G. Grushin, *et al.*, *Nat. Commun.* **7** (2016).
- <sup>26</sup> J. Liu, J. Hu, Q. Zhang, D. Graf, H. B. Cao, S. Radmanesh, D. Adams, Y. Zhu, G. Cheng, X. Liu, *et al.*, *Nat. Mater.* **16**, 905 (2017).
- <sup>27</sup> S. Borisenko, D. Evtushinsky, Q. Gibson, A. Yaresko, T. Kim, M. Ali, B. Buechner, M. Hoesch, and R. J. Cava, arXiv preprint arXiv:1507.04847 (2015).
- <sup>28</sup> Y.-Y. Wang, S. Xu, L.-L. Sun, and T.-L. Xia, *Phys. Rev. Mater.* **2**, 021201 (2018).
- <sup>29</sup> R. Kealhofer, S. Jang, S. M. Griffin, C. John, K. A. Benavides, S. Doyle, T. Helm, P. J. Moll, J. B. Neaton, J. Y. Chan, *et al.*, *Phys. Rev. B* **97**, 045109 (2018).
- <sup>30</sup> G. Bian, T.-R. Chang, R. Sankar, S.-Y. Xu, H. Zheng, T. Neupert, C.-K. Chiu, S.-M. Huang, G. Chang, I. Belopolski, *et al.*, *Nat. Commun.* **7**, 10556 (2016).
- <sup>31</sup> Q. Xu, Z. Song, S. Nie, H. Weng, Z. Fang, and X. Dai, *Phys. Rev. B* **92**, 205310 (2015).
- <sup>32</sup> J. Hu, Z. Tang, J. Liu, X. Liu, Y. Zhu, D. Graf, K. Myhro, S. Tran, C. N. Lau, J. Wei, *et al.*, *Phys. Rev. Lett.* **117**, 016602 (2016).
- <sup>33</sup> N. Kumar, K. Manna, Y. Qi, S.-C. Wu, L. Wang, B. Yan, C. Felser, and C. Shekhar, *Phys. Rev. B* **95**, 121109 (2017).
- <sup>34</sup> A. Burkov, M. Hook, and L. Balents, *Phys. Rev. B* **84**, 235126 (2011).
- <sup>35</sup> Y.-Y. Wang, Q.-H. Yu, P.-J. Guo, K. Liu, and T.-L. Xia, *Phys. Rev. B* **94**, 041103 (2016).
- <sup>36</sup> D. Wu, J. Liao, W. Yi, X. Wang, P. Li, H. Weng, Y. Shi, Y. Li, J. Luo, X. Dai, *et al.*, *Appl. Phys. Lett.* **108**, 042105 (2016).
- <sup>37</sup> Z. Yuan, H. Lu, Y. Liu, J. Wang, and S. Jia, *Phys. Rev. B* **93**, 184405 (2016).
- <sup>38</sup> B. Shen, X. Deng, G. Kotliar, and N. Ni, *Phys. Rev. B* **93**, 195119 (2016).
- <sup>39</sup> Y. Luo, R. McDonald, P. Rosa, B. Scott, N. Wakeham, N. Ghimire, E. Bauer, J. Thompson, and F. Ronning, *Sci Rep* **6**, 27294 (2016).
- <sup>40</sup> Y. Li, L. Li, J. Wang, T. Wang, X. Xu, C. Xi, C. Cao, and J. Dai, *Phys. Rev. B* **94**, 121115 (2016).
- <sup>41</sup> P.-J. Guo, H.-C. Yang, B.-J. Zhang, K. Liu, and Z.-Y. Lu, *Phys. Rev. B* **93**, 235142 (2016).
- <sup>42</sup> R. Lou, Y. Xu, L.-X. Zhao, Z.-Q. Han, P.-J. Guo, M. Li, J.-C. Wang, B.-B. Fu, Z.-H. Liu, Y.-B. Huang, *et al.*, *Phys. Rev. B* **96**, 241106 (2017).
- <sup>43</sup> P. E. Blöchl, *Phys. Rev. B* **50**, 17953 (1994).
- <sup>44</sup> G. Kresse and D. Joubert, *Phys. Rev. B* **59**, 1758 (1999).
- <sup>45</sup> G. Kresse and J. Hafner, *Phys. Rev. B* **47**, 558 (1993).
- <sup>46</sup> G. Kresse and J. Furthmüller, *Comp. Mater. Sci.* **6**, 15 (1996).
- <sup>47</sup> G. Kresse and J. Furthmüller, *Phys. Rev. B* **54**, 11169 (1996).
- <sup>48</sup> J. P. Perdew, K. Burke, and M. Ernzerhof, *Phys. Rev. Lett.* **77**, 3865 (1996).
- <sup>49</sup> N. Marzari and D. Vanderbilt, *Phys. Rev. B* **56**, 12847 (1997).

- <sup>50</sup> I. Souza, N. Marzari, and D. Vanderbilt, *Phys. Rev. B* **65**, 035109 (2001).
- <sup>51</sup> G. J. Miller, F. Li, and H. F. Franzen, *J. Am. Chem. Soc.* **115**, 3739 (1993).
- <sup>52</sup> H. Zogg and P. Schwelling, *J. Mater. Sci.* **14**, 1923 (1979).
- <sup>53</sup> D. Chen, L. Zhao, J. He, H. Liang, S. Zhang, C. Li, L. Shan, S. Wang, Z. Ren, C. Ren, *et al.*, *Phys. Rev. B* **94**, 174411 (2016).
- <sup>54</sup> R. H. McKenzie, J. Qualls, S. Han, and J. Brooks, *Phys. Rev. B* **57**, 11854 (1998).
- <sup>55</sup> D. Shoenberg, *Magnetic oscillations in metals* (Cambridge University Press, 2009).
- <sup>56</sup> A. Kokalj, *Comp. Mater. Sci.* **28**, 155 (2003).